Supporting Information

Enhanced performance of $Pr_4Ni_3O_{10\pm\delta}$ - $Ce_{0.75}Gd_{0.1}Pr_{0.15}O_{2-\delta}$ composite electrode via particle size grading

Zheng Xie[1], Yasmine Baghdadi[2], and Stephen J Skinner*[1,3]

[1]Department of Materials, Imperial College London, Exhibition Road, London, SW7 2AZ, UK
[2]Department of Chemical Engineering, Imperial College London, Exhibition Road, London, SW7 2AZ, UK
[3]International Institute for Carbon Neutral Energy Research, Kyushu University, Japan

S1 Supporting data

S1.1 X-ray diffraction

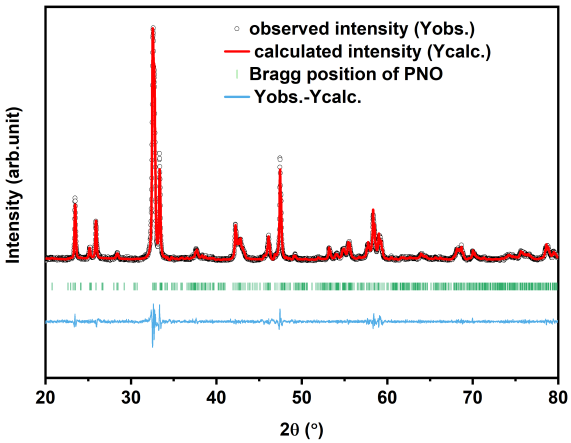

Figure S1: The XRD pattern of (a) unmilled PNO with lattice parameters of a= 5.3752(1) Å, b= 5.4635(1) Å, c= 27.5479(6) Å, $\beta = 90.317(2)°$. The χ^2 was 1.86.

*Corresponding author. Tel.: +44 (0)20 7594 6782
Email address: s.skinner@imperial.ac.uk (S.J. Skinner)

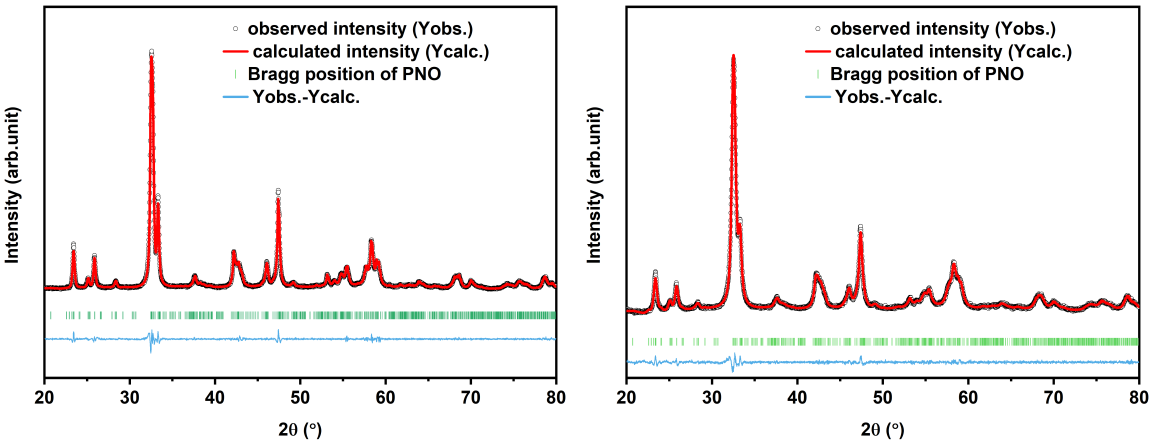

(a) (b)

Figure S2: XRD patterns of (a) milled PNO with lattice parameter a= 5.3761(2) Å, b= 5.4653(2) Å, c= 27.5482(5) Å, $\beta = 90.372(2)°$, (b) twice-milled PNO with lattice parameters of a= 5.3846(2) Å, b= 5.4734(2) Å, c= 27.5612(4) Å, $\beta = 90.456(3)°$. The χ^2 was 1.98 and 1.32, respectively.

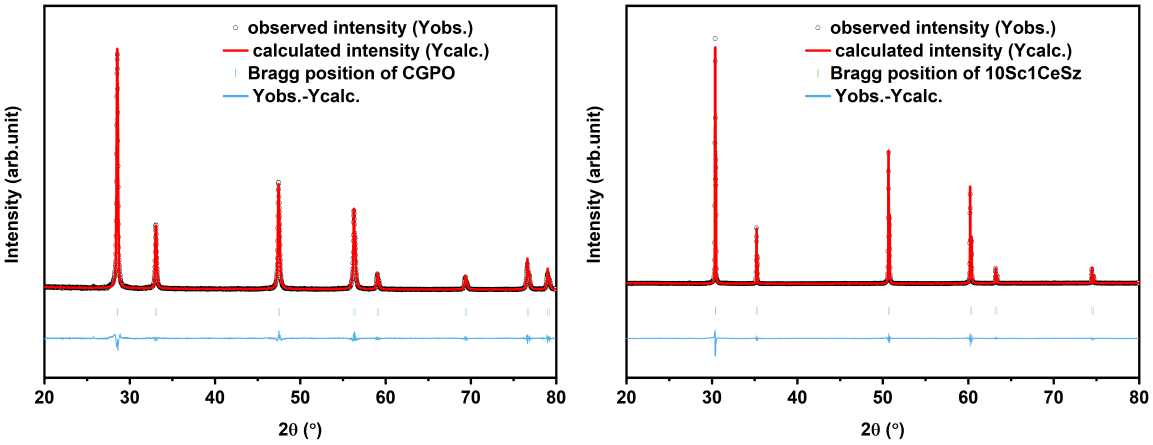

(a) (b)

Figure S3: XRD patterns of (a) as prepared CGPO with lattice parameters of a=b=c= 5.4163(1) Å, (b) pellet attached with the interlayer with lattice parameter a=b=c=5.0923 (1) Å. The χ^2 was 1.17 and 1.91, respectively.

The electrode was removed from the pellet for characterization otherwise the signal from the electrolyte was too strong to see the signal from the electrode. Since the electrode was very thin so the amount of powder obtained from a symmetrical cell was less, and considering the change in particle size (from the micron scale to semi-micron scale) of PNO would not affect its reactivity, the electrode of all investigated symmetrical cells was mixed for XRD characterization. There were signals from gold and 10Sc1CeSz because the gold and 10Sc1CeSz from the interlayer were mixed with electrodes during removing electrodes from pellets.

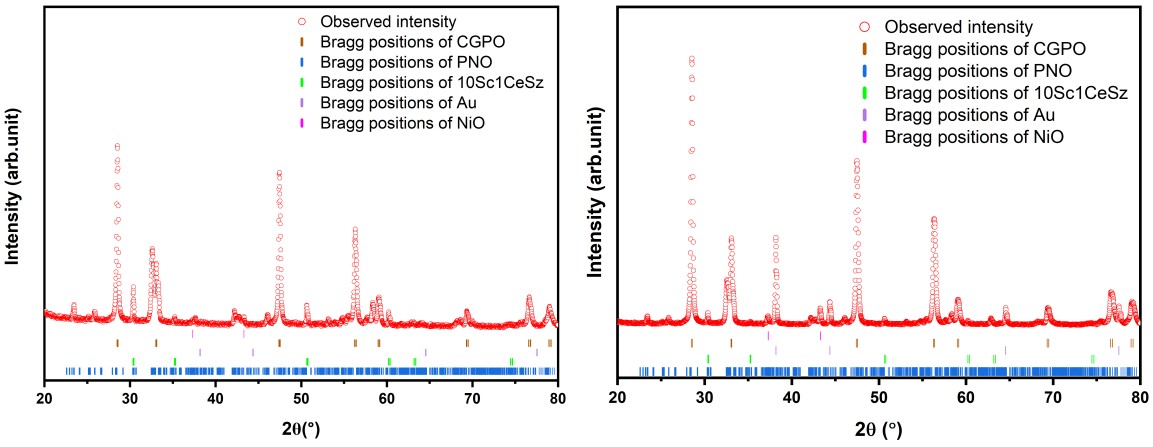

(a) (b)

Figure S4: XRD patterns of (a) electrodes before impedance measurements, and (b) electrodes after impedance measurements.

S1.2 Brunauer-Emmett-Teller

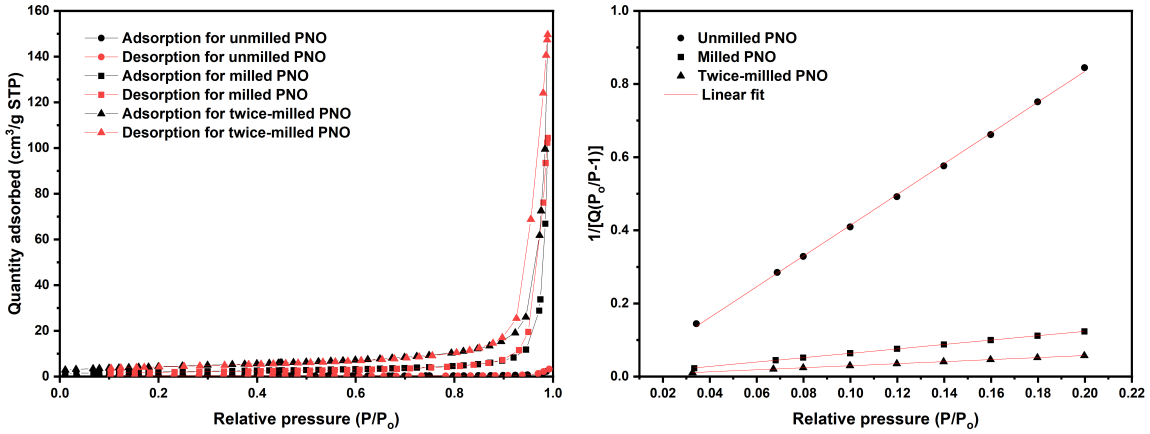

(a) (b)

Figure S5: (a) Isotherm linear plot and (b) BET surface area plot, for three PNO powders.

S1.3 Focused ion beam - scanning electron microscopy

Electrode	S_{UM}^{UM}	S_{M}^{M}	S_{MM}^{MM}
Average particle size PNO (nm)	1240 ± 40	504 ± 46	313 ± 25
Average particle size Pore(nm)	55 ± 5	46 ± 10	54 ± 5
Average particle size CGPO(nm)	46 ± 6	42 ± 14	48 ± 1
Total TPB density(um^{-2})	5.1 ± 0.5	7.0 ± 1.2	10.0 ± 1.6
Active TPB density(um^{-2})	4.6 ± 0.1	6.6 ± 1.2	9.1 ± 1.5
Total DPB density(um^{-1})	145 ± 17	222 ± 33	273 ± 61
Active DPB density(um^{-1})	138 ± 21	212 ± 39	263 ± 67
Tortuosity of PNO	19 ±1	40 ± 7	50 ± 5
Tortuosity of CGPO	2.3 ± 0.2	3.3 ± 0.5	5.5 ± 0.9

Table S1: Microstructural parameters for electrodes without particle size grading. The tortuosity data was obtained from Taufactor [1] and the rest of the data were extracted from Avizo [2].

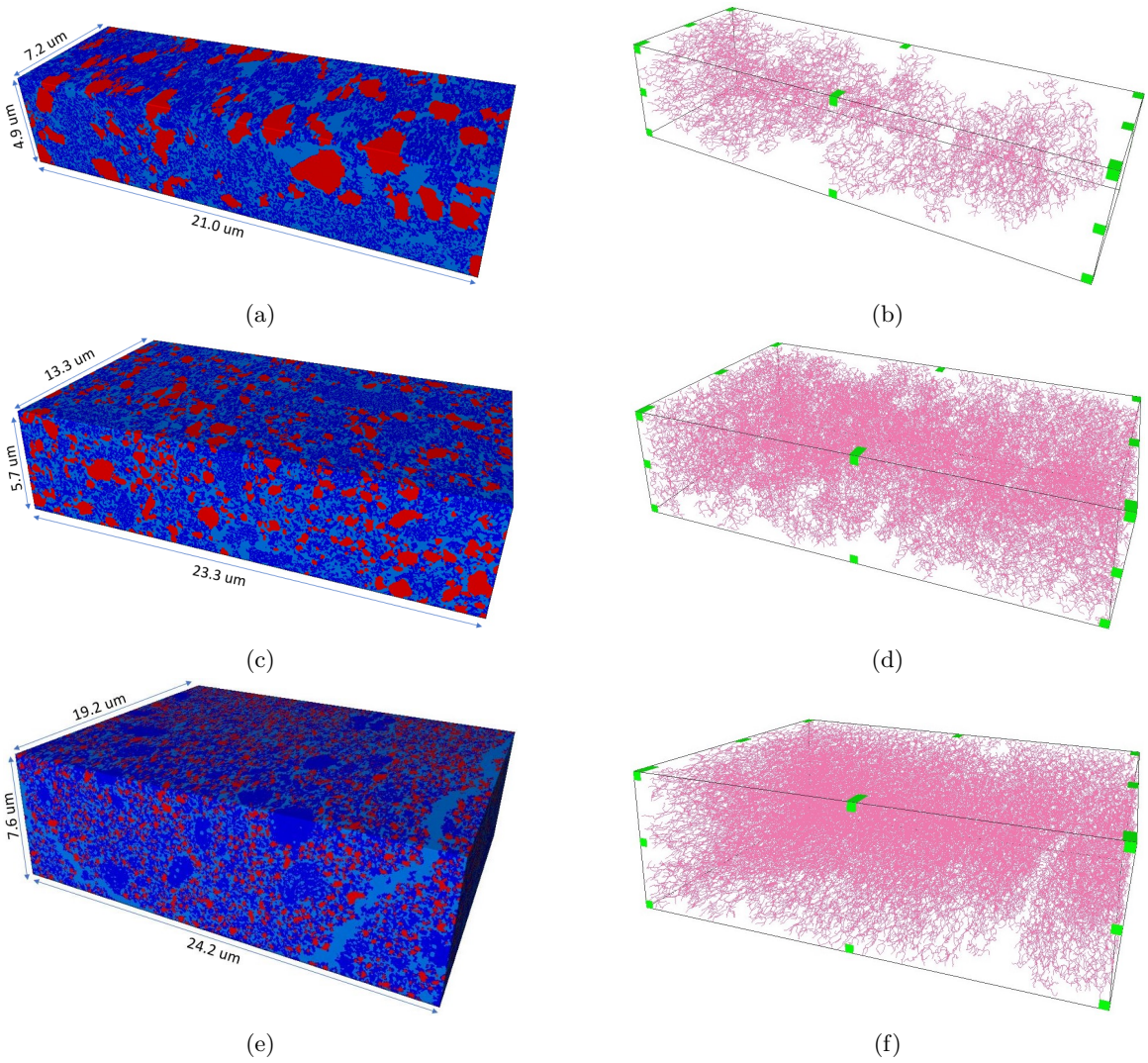

Figure S6: 3D volume-rendering of analyzed sample volume for the electrode (a) S_{UM}^{UM}, (c) S_{M}^{M}, (e) S_{MM}^{MM} (Red phase represents PNO, light and dark blue phases represent pore and CGPO, respectively and corresponding active triple phase boundary skeleton network in (b), (d), and (f), respectively, reproduced from [2] under a CC BY 4.0 license.

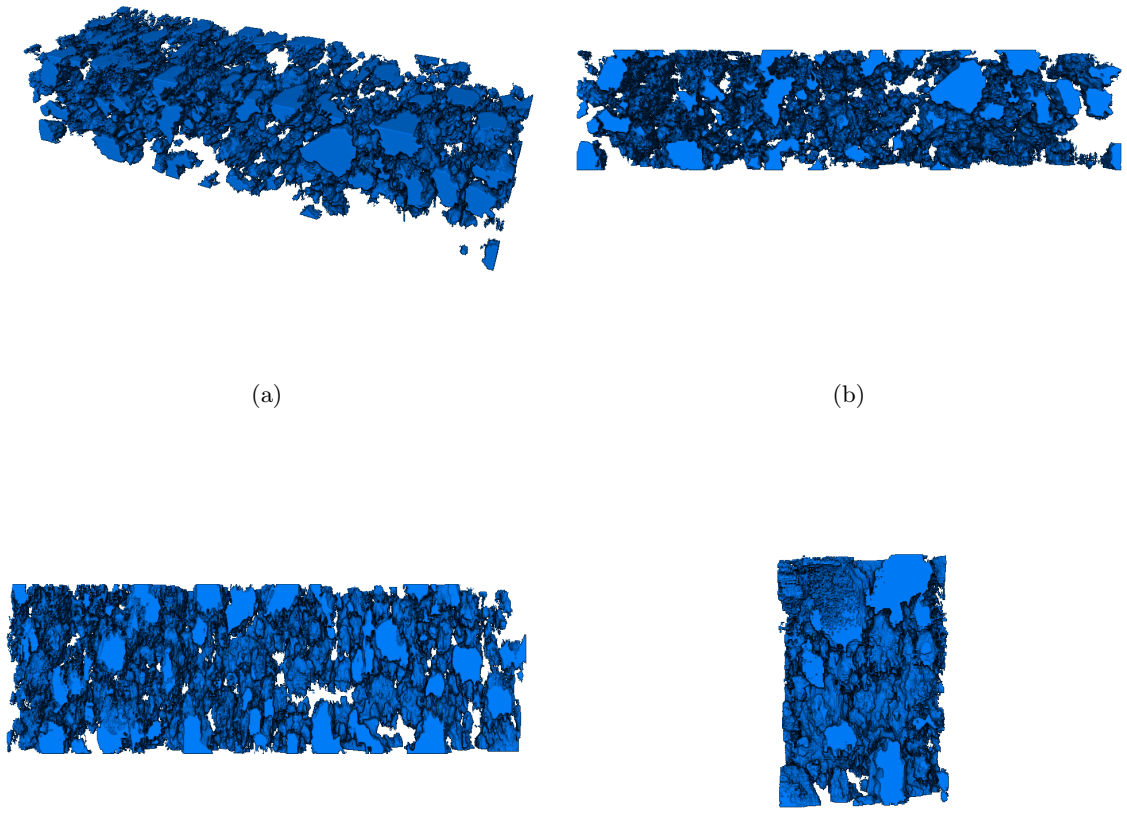

(a) (b)

(c) (d)

Figure S7: The image of unmilled PNO distribution in 3D space with (a)3/4 view, (b) front view, (c) top view and (d) side view.

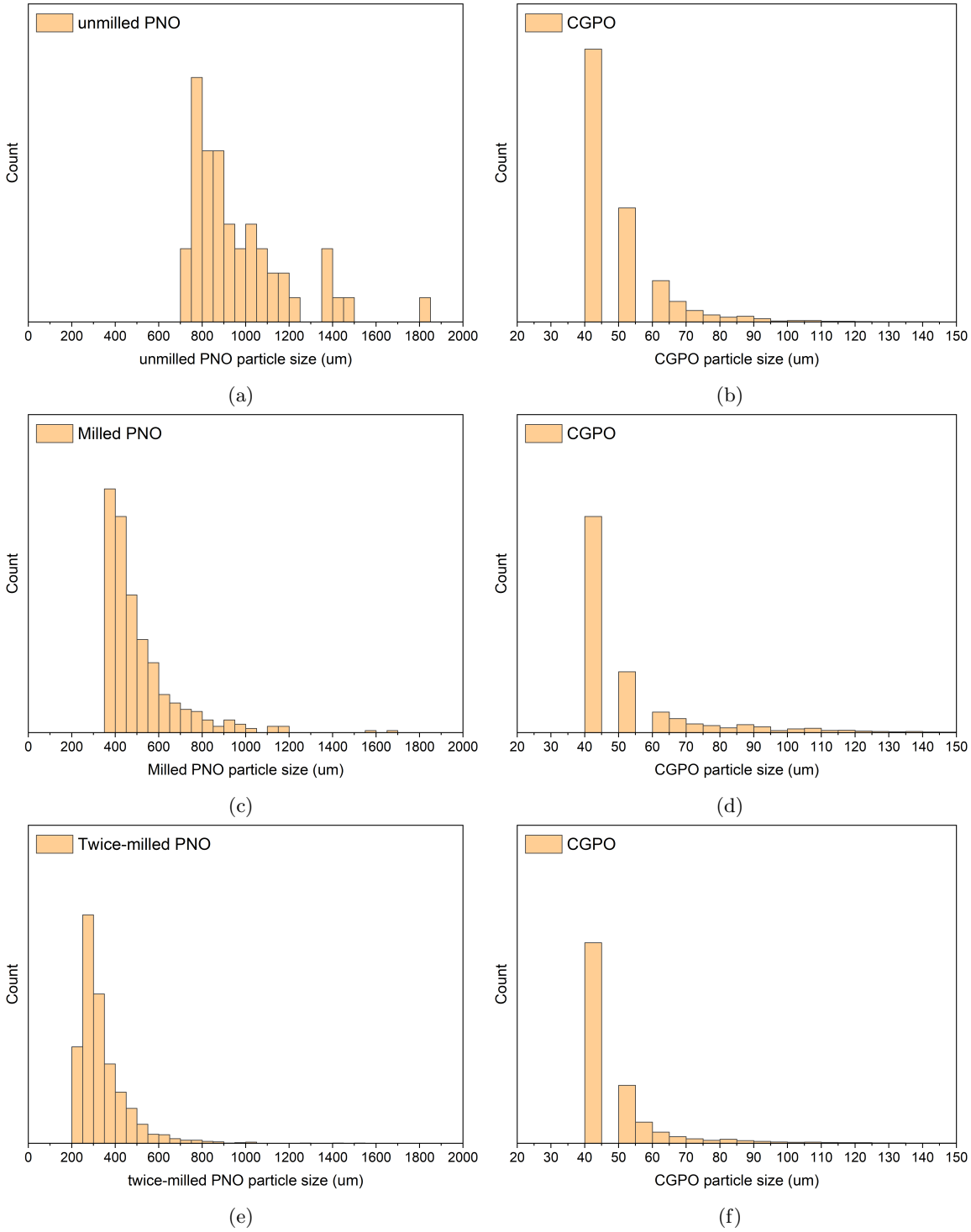

Figure S8: Particle size distribution of (a) unmilled PNO and (b) CGPO in the electrode composed of unmilled PNO and CGPO, and that of (c) milled PNO and (d) CGPO in the electrode composed of milled PNO and CGPO, and that of (e) twice-milled PNO and (f) CGPO in the electrode composed of twice-milled PNO and CGPO

S1.4 Electrochemical impedance spectroscopy

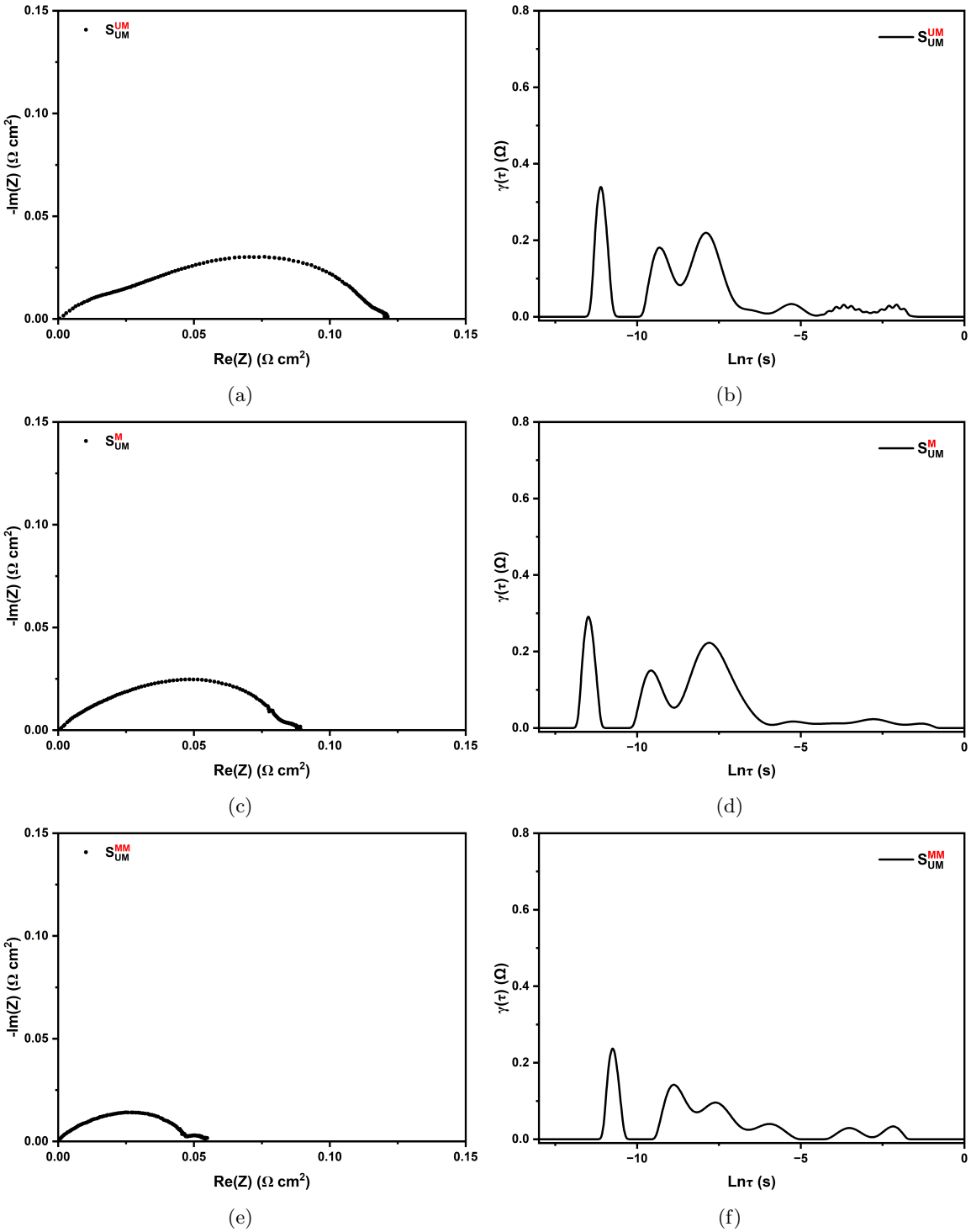

Figure S9: The Nyquist plot of (a) S^{UM}_{UM}, (c) S^{M}_{UM} and (e) S^{MM}_{UM} at 625 $^{\circ}C$ at pO_2 of 0.21 atm, and their corresponding DRT spectrum at (b), (d) and (f), respectively.

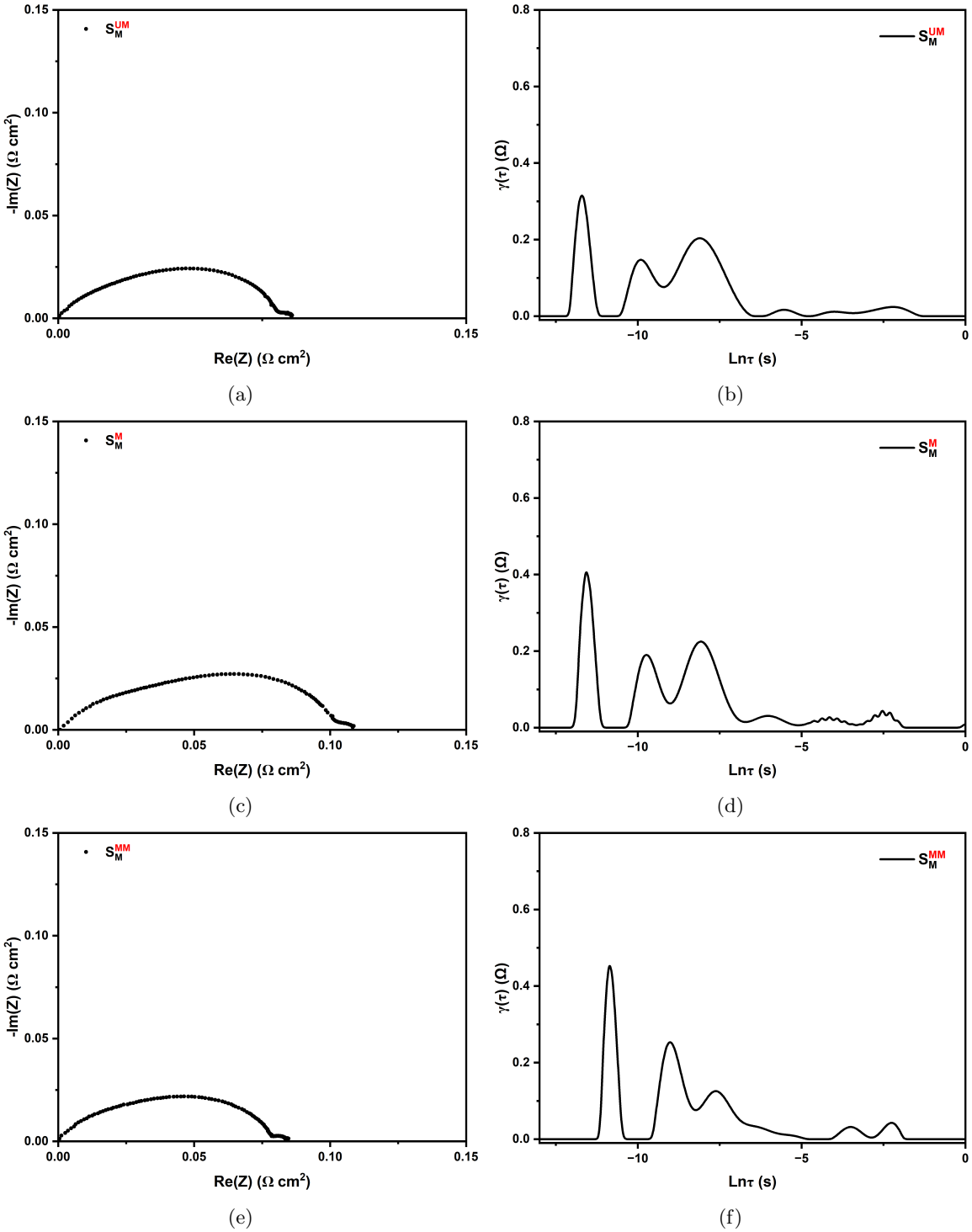

Figure S10: The Nyquist plot of (a) S_M^{UM}, (c) S_M^M and (e) S_M^{MM} at 625 $^\circ C$ at pO_2 of 0.21 atm, and their corresponding DRT spectrum at (b), (d) and (f), respectively.

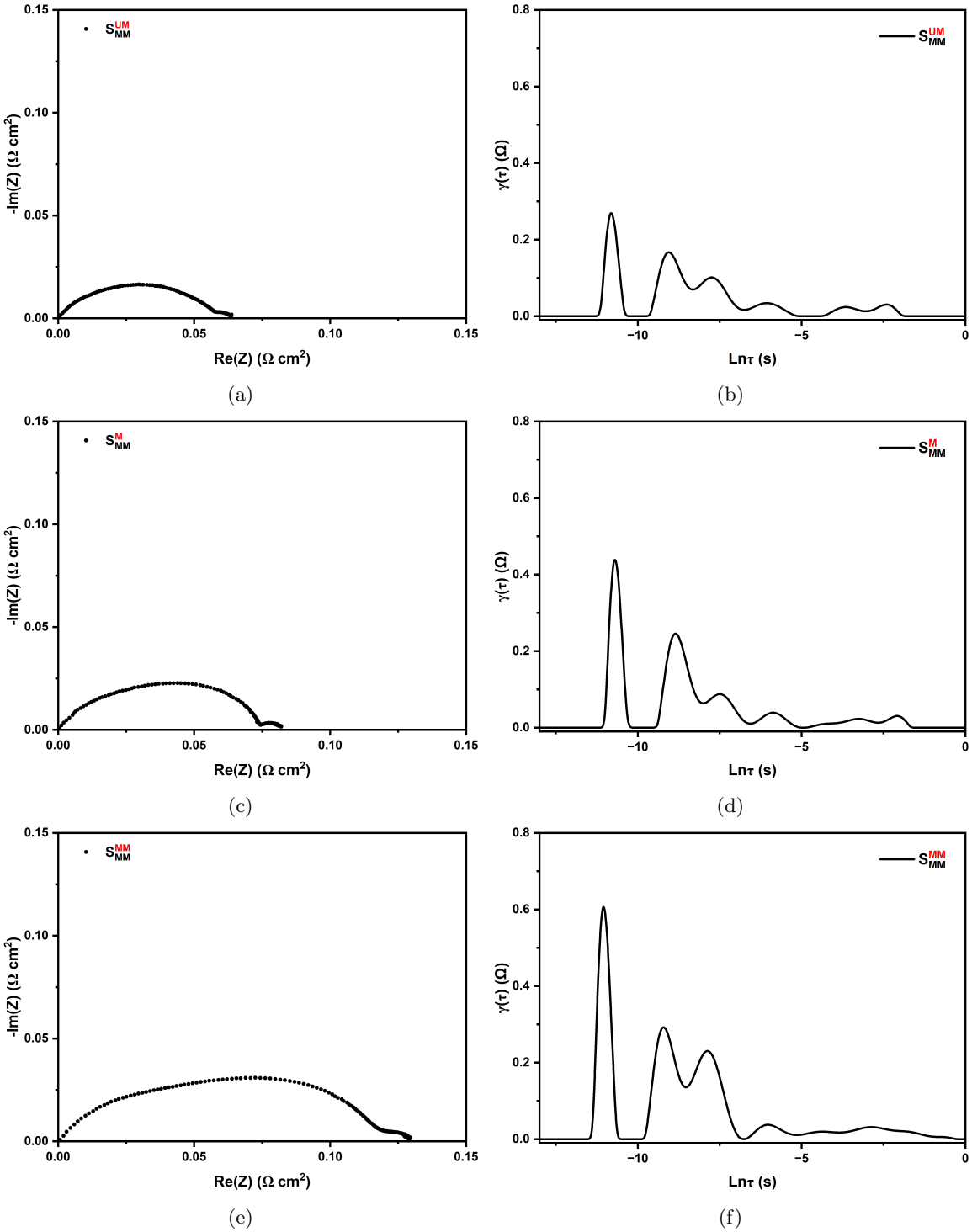

Figure S11: The Nyquist plot of (a) S^{UM}_{MM}, (c) S^{M}_{MM} and (e) S^{MM}_{MM} at 625 $^{\circ}C$ at pO_2 of 0.21 atm, and their corresponding DRT spectrum at (b), (d) and (f), respectively.

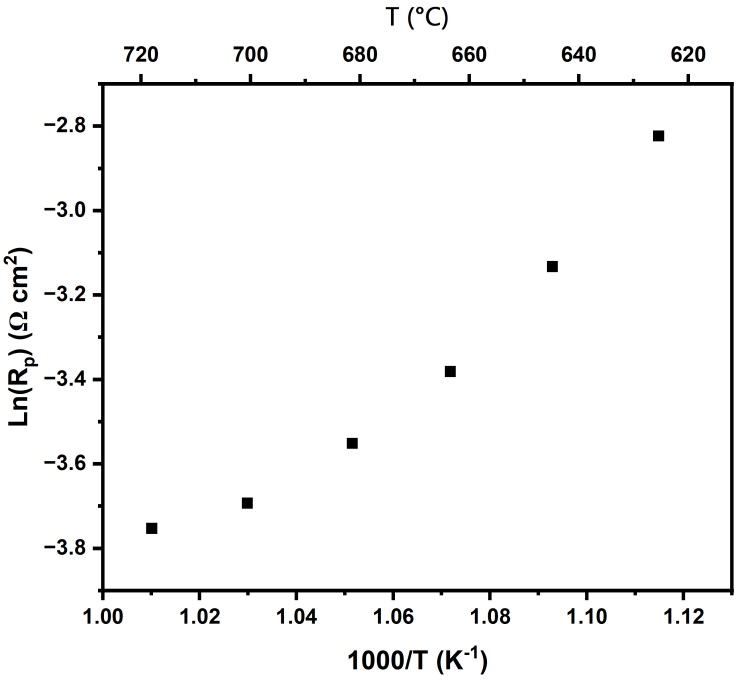

Figure S12: Arrhenius plot of the total polarization resistance of the electrode S_{UM}^{MM} at pO_2 of 0.21 *atm* from 625 °*C* to 717 °*C*.

References

(1) Cooper, S. J.; Bertei, A.; Shearing, P. R.; Kilner, J. A.; Brandon, N. P. *SoftwareX* **2016**, *5*, 203–210, DOI: 10.1016/j.softx.2016.09.002.

(2) Xie, Z.; Jang, I.; Ouyang, M.; Hankin, A.; Skinner, S. *Journal of Physics: Energy* **2023**, *5*, 045005, DOI: 10.1088/2515-7655/aceeb5.